ACS Catalysis

Research Article

pubs.acs.org/acscatalysis

Insight into the Balancing Effect of Active Cu Species for Hydrogenation of Carbon−Oxygen Bonds

Yue Wang, Yongli Shen, Yujun Zhao, Jing Lv, Shengping Wang, and Xinbin Ma*

Key Laboratory for Green Chemical Technology of Ministry of Education, Collaborative Innovation Centre of Chemical Science and Engineering, School of Chemical Engineering and Technology, Tianjin University, Tianjin 30072, People's Republic of China

Supporting Information

ABSTRACT: Hydrogenation of carbon−oxygen (C−O) bonds plays a significant role in organic synthesis. Cu-based catalysts have been extensively investigated because of their high selectivity in C−O hydrogenation. However, no consensus has been reached on the precise roles of Cu^0 and Cu^+ species for C−O hydrogenation reactions. Here we resolve this long-term dispute with a series of highly comparable Cu/SiO_2 catalysts. All catalysts represent the full-range distribution of the Cu species and have similar general morphologies, which are detected and mutually corroborated by multiple characterizations. The results demonstrate that, when the accessible metallic Cu surface area is below a certain value, the catalytic activity of hydrogenation linearly increases with increasing Cu^0 surface area, whereas it is primarily affected by the Cu^+ surface area. Furthermore, the balancing effect of these two active Cu sites on enhancing the catalytic performance is demonstrated: the Cu^+ sites adsorb the methoxy and acyl species, while the Cu^0 facilitates the H_2 decomposition. This insight into the precise roles of active species can lead to new possibilities in the rational design of catalysts for hydrogenation of C−O bonds.

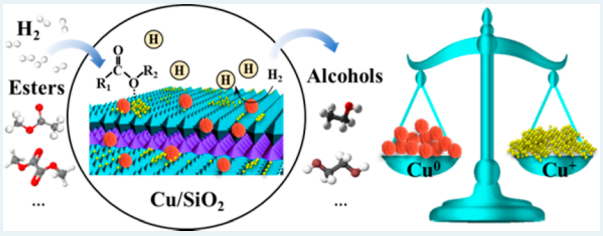

KEYWORDS: *Cu catalyst, hydrogenation, Cu^0/Cu^+ active sites, methyl acetate, alcohol, balancing effect*

INTRODUCTION

Hydrogenation of C−O bonds (e.g., esters, carboxylic acids, ethers, furfural, and CO_2) is a powerful tool in organic synthesis.[1−4] It can generate a variety of attractive products with numerous commercial applications (chemical feedstocks, fuel alternatives or additives, polymers, etc.).[5,6] However, in the hydrogenation process, hydrogenolysis occurs at both the C−O bond (forming alcohols) and the C−C bond (forming low-molecular-weight components such as CH_4, CO, and CO_2). In comparison with other transition metals or oxides,[7,8] Cu species are considered as excellent catalytically active sites accounting for the selective hydrogenation of C−O bonds and are relatively inactive toward C−C bond hydrogenolysis, which have been widely used in vapor-phase chemoselective hydrogenation reactions.[9−11]

Significant advancements in preparing efficient and stable Cu-based catalysts have been achieved in the past decade, as well as a preliminary understanding of the catalytic essence of the hydrogenation reactions. Regarding extensive investigations on silica carrier supported Cu catalysts, the Cu dispersion or/and interaction between the Cu species and the support or promoter are believed to be pivotal in determining the catalytic activity and stability. However, concerning the nature of active species, no consensus has been reached on the precise roles of Cu^0 and Cu^+ species for hydrogenation reactions. Several researchers have contradictory opinions about the proper surface distribution of Cu^0 and Cu^+ sites that most benefits the catalytic performance.

In an earlier study, San et al.[12] considered only Cu^0 species to be active sites in the hydrogenation reaction. However, the synergetic effect between Cu and the oxide components has been proposed to enhance the catalytic performance toward the hydrogenation of methyl acetate (MA),[13] dimethyl oxalate (DMO),[14,15] furfural,[10] and CO_2[16] and has been supported by numerous subsequent studies. Although the cooperation of Cu^0 and Cu^+ species in C−O hydrogenation has been mostly confirmed, their respective contributions to the catalytic activity remain in dispute.

Some researchers have proposed that metallic Cu is the primary active site, because the catalytic activity has been frequently observed to be proportional to the Cu^0 specific surface area ($S_{Cu(0)}$). For example, numerous works on Cu/SiO_2,[17] Cu/HMS,[18,19] and $Cu/SiO_2−TiO_2$[20] catalysts by Dai et al. have supported this view and reported catalysts with the maximum ratio of Cu^0/Cu^+ had the highest catalytic activity in DMO hydrogenation. Furthermore, our previous studies revealed a strong correlation between the density of surface Cu^0 sites and the formation rate of alcohols, which indicated that Cu^0 was the active site.[14,21] Simultaneously, no clear relationship was observed between the activity and the number of Cu^+ sites. In contrast, Yuan and co-workers suggested that a high proportion of Cu^+/Cu^0 should be a key prerequisite to

Received: August 2, 2015
Revised: September 13, 2015
Published: September 14, 2015

DOI: 10.1021/acscatal.5b01678
ACS Catal. 2015, 5, 6200−6208

obtaining outstanding hydrogenation performance; this suggestion was also based on extensive experimental data. The catalytic activity and stability of Cu/SiO_2 was remarkably increased after modified with B,[22] La,[23] Ag,[24] and Au,[25] which essentially minimized the reducibility of cuprous species or increased the Cu^+ surface concentration. These studies demonstrated that Cu^+ species acted as efficient active sites to activate the ester groups. Thus, a deeper understanding of the contributions of Cu species to the reaction is necessary for more rational catalyst design.

On comparison of the available literature, it is found that the catalysts were prepared using different methods and exhibited different distributions of Cu species. In particular, the Cu^0 surface areas varied over completely different ranges: one range of $S_{Cu(0)}$ varies from 1.6 to 11.7 m^2/g,[17−20] whereas another varies from 21.3 to 49.1 m^2/g.[22−25] Notably, this discrepancy in the Cu^0 surface areas is likely responsible for the two aforementioned contradictory conclusions on the contributions of Cu species. Therefore, to settle the debate and comprehensively elucidate the roles and the balancing effect of Cu^0 and Cu^+ sites in catalytic hydrogenation, the controlled preparation of catalysts with both similar general morphology and full-range distribution of Cu species is imperative.

The ammonia evaporation method can conveniently and effectively disperse Cu species on silica and form strong metal−support interactions, thereby guaranteeing the formation of both Cu^0 and Cu^+ species.[26] Thus, this method was used in this work and we obtained a series of Cu/SiO_2 catalysts with both highly similar textures and substantially different distributions of Cu species, which enabled us to elucidate the precise roles of the active sites.

EXPERIMENTAL SECTION

Materials. All chemicals were handled in air and used as received. $Cu(NO_3)_2{\cdot}3H_2O$ (99%) and aqueous ammonia solution (25−28 wt %) were purchased from Sinopharm Chemical Reagent Co. Silica sol (30 wt %) was purchased from Qingdao Grand Chemical Co. Deionized water (18.2 MΩ) was used in all syntheses. Ethanol (99.5 wt %) used to wash the precipitate was purchased from Tianjin Kemiou Chemical Reagent Co.

Catalyst Synthesis. The Cu/SiO_2 catalysts were prepared by the ammonia evaporation method, briefly described as follows. For example, to prepare the 20 wt % Cu loading catalyst, 15.2 g of $Cu(NO_3)_2{\cdot}3H_2O$ was dissolved in 100 mL of deionized water and 50 mL of aqueous ammonia solution. After the mixture was stirred for 15 min, 45 mL of silica sol was added dropwise to the copper−ammonia complex solution and stirred for several hours at room temperature. This procedure made the raw materials interact with each other (denoted as the aging process). The aging time became one of the significant factors in catalyst preparation. *n*Cu-*x*h denotes the Cu/SiO_2 catalysts with *n* wt % Cu loading and *x* hours of aging time. After that, the suspension was heated in a 353 K water bath to start ammonia evaporation. This process was terminated when the pH value reached 6−7. The precipitate was separated through filtration, washed with water and ethanol, and then dried under vacuum at 353 K overnight. The resulting solid was calcined in static air at 673 K for 4 h, tableted, crushed, and sieved to 40−60 mesh.

The preparation for treatment of silica sol with ammonia solely as the aging process is as follows. The silica sol was first stirred with aqueous ammonia solution at 303 and 353 K, respectively, for 4 h as the aging procedure. After the 50 mL solution of $Cu(NO_3)_2{\cdot}3H_2O$ was added, the mixture was heated in a 353 K water bath to allow the evaporation of ammonia. The following steps of preparation were the same as those described previously. These two kinds of catalysts are denoted as *n*Cu-303-4h and *n*Cu-353-4h correspondingly.

Catalyst Characterization. N_2 adsorption/desorption analysis was conducted at 77 K using a Micromeritics Tristar 3000 apparatus. The specific surface area was calculated from the isotherms by the Brunauer−Emmett−Teller (BET) method, and the pore size distribution was calculated by the Barrett−Joyner−Halenda (BJH) method from the desorption isotherms.

An inductively coupled plasma optical emission spectrometer (ICP-OES, Varian Vista-MPX) was used to analyze the Cu content of samples. The peak at 324.754 nm was used as the Cu characteristic wavelength to identify the Cu^{2+} concentration of samples.

Transmission electron microscopy (TEM) images were obtained with a Philips TECNAI G2 F20 system electron microscope equipped with a field emission gun. The samples were made by dropping catalyst powders in ethanol solution after they were ground and ultrasonic dispersion onto the carbon-coated molybdenum grids.

X-ray diffraction (XRD) patterns for the catalyst were obtained on a Rigaku C/max-2500 diffractometer employing the graphite-filtered Cu Kα radiation (λ = 1.5406 Å) at room temperature. Data were acquired by scanning at a rate of 8°/min from 2θ = 10−90°. To obtain accurate information, the samples were reduced just before XRD analysis and sealed into glass bottles filled with Ar. The Scherrer equation was used to calculate the particle size of Cu species.

X-ray photoelectron spectra (XPS) and Auger electron spectroscopy (XAES) were carried out on a PHI 1600 ESCA instrument (PE Company) equipped with an Al Kα X-ray radiation source ($h\nu$ = 1486.6 eV). To obtain accurate information on the surface states of Cu species in reduced catalysts, the samples were collected by the following procedures. The catalysts were pressed into thin disks and reduced under a flow of H_2 at 623 K for 4 h. After they were cooled to room temperature, the samples were placed into centrifuge tubes and sealed with Ar. Then the samples were transferred to the holder in less than 5 min and outgassed in the chamber. The analyses were taken under a vacuum of 1×10^{-8} Torr. The binding energies were calibrated using the Si 2p peak at 103.2 eV as the reference. The experimental errors were within ±0.2 eV.

The Cu dispersion and the specific surface area of metallic Cu species was measured by the N_2O chemisorption and hydrogen pulse reduction method (N_2O titration) using a Micromeritics Autochem II 2920 apparatus. Briefly, after pretreatment with He at 473 K for 1 h, 50 mg of the catalysts was reduced under a flow of H_2 at 623 K for 2 h and cooled to 363 K. The pure N_2O was induced at a rate of 30 mL/min for 1 h, ensuring that surface Cu atoms were completely oxidized to Cu_2O. Then hydrogen pulse reduction of surface Cu_2O to metallic Cu was conducted at 623 K and repeated until the pulse area no longer changed. The consumed amount of hydrogen was the value obtained by subtracting the amount of residual H_2 calculated from the areas shown in TCD signals from the total amount of H_2 pulsed. From that, the surface metallic Cu areas of catalysts could be calculated. In

DOI: 10.1021/acscatal.5b01678
ACS Catal. 2015, 5, 6200−6208

combination with the ICP results, we could obtain the metallic Cu dispersion as well.

The in situ FTIR of CO adsorption was performed to determine the amount of active surface Cu(I) species of samples. A Nicolet 6700 spectrometer equipped with a MCT/A detector and a vacuum system was used. The samples were self-supporting disks that were formed by pressing 20 mg of finely ground dried catalysts at 8 MPa. Then the disk was weighed again before it was settled into an in situ cell which allowed the possibility of high temperature experiments that was connected with a vacuum-adsorption system. The sample disk was reduced and then was cooled to 303 K under a high-purity He flow. After background collection, the sample was exposed and scanned to the flow of CO at 303 K for 30 min. Then the sample was vacuumed and scanned. The last spectrum was confirmed to be no different from the previous one. For normalization, the intensity of the spectrum was enlarged by the same multiple as the disk weight used to be enlarged to 1 g. Therefore, the areas under the peaks in the normalized spectra could give a qualitative estimate of the amount of certain species, since the extinction coefficients of the corresponding IR bands are not known.

The in situ FTIR of methanol adsorption was also carried out with a Nicolet 6700 spectrometer. The sample disks after reduction were exposed to a gas mixture of He and CH_3OH at 300 K for 30 min. To guarantee that methanol was absorbed as a monolayer on the surface active sites of catalysts, the desorption was performed under vacuum at 300 K and the spectra were programmed to be scanned. After the desorption spectra no longer changed, the temperature was raised up to 488 K, the reaction temperature, to obtain another desorption spectrum which would help to distinguish the different methanol adsorption strengths on different surface active sites of catalysts. Deconvolution of the final spectra allowed us to qualitatively estimate the amount of certain species by integration of the areas under corresponding IR peaks.

Catalytic Activity Evaluation and Product Analysis. The catalytic activity evaluations were carried out with a continuous-flow heterogeneous reactor. Samples of 0.5 g of the catalysts (40−60 mesh) were placed carefully into a certain part of the tube with maintenance of a constant temperature and ensured to be smooth with a low ratio of voids. The reaction tests were carried out at 488 K on 2.5 MPa with 80 as the charge-in molar ratio of H_2 to MA after the catalysts were reduced at the flow rate of 100 mL/min of hydrogen at 623 K for 4 h. The products were condensed and analyzed with an Agilent Micro GC 6820 instrument with an HP-INNOWAX capillary column (Hewlett-Packard, 30 m × 0.32 mm × 0.50 μm). The main byproducts include methanol, ethyl acetate, *n*-propanol, 2-butanol, acetaldehyde, etc. The $TOF_{Cu(0)}$ values were calculated on the basis of metallic Cu dispersion. Assuming that the Cu^+ ion occupies the same area as that of the Cu^0 atom, the $TOF_{Cu(I)}$ values were calculated by dispersion on the basis of $S_{Cu(I)}$.

RESULTS

Textural and Morphological Properties of the Catalysts. To investigate the contributions of Cu species to the reaction, other factors (e.g., pore structure and size of the metal particles) should first be excluded. As shown in Table 1, all catalysts have relatively high Brunauer−Emmett−Teller (BET) specific surface areas and parallel mesoporous structures. Moreover, the transmission electron microscopy (TEM) images (Figure 1) indicate that all of the reduced catalysts have similar morphologies and that the Cu is well dispersed. The observed metallic Cu grains on the surface are <5 nm, even those on the surface of a catalyst with up to 40 wt % Cu. This grain size is also confirmed by the X-ray diffraction (XRD) patterns of the reduced catalysts (Figure 2), which show extremely weak and broad diffraction peaks at 2θ angles of 43.3 and 36.4°; these peaks are attributed to metallic Cu(111) (JCPDS 04-0836) and Cu_2O(111) planes (JCPDS 65-3288), respectively. No obvious diffraction peaks of other crystal faces are observed, which strongly implies that the Cu species is highly dispersed on SiO_2 supports. Meanwhile, the sizes of Cu nanoparticles calculated using the Scherrer formula are also notably small, consistent with the results from the TEM images (given in Table 1). In addition, the XRD peaks assigned to the Cu_2O(111) plane suggest that a portion of Cu exists as Cu^+ after reduction. Given the above results, the textural and physicochemical structures of the Cu/SiO_2 catalysts are so similar that these factors are negligible in the following discussion, which enables the further exploration of the active species contributions.

Table 1. Textural and Physicochemical Properties of Reduced Cu/SiO_2 Catalysts

catalyst	metal loading (wt %)[a]	S_{BET} (m^2/g)	D_{pore} (nm)	crystallite size (nm) by XRD[b]	crystallite size (nm) by TEM
5Cu-303-4h	4.9	254	10.4	ND[c]	2.6
5Cu-353-4h	5.0	250	11.7	ND	2.3
5Cu-4h	5.0	263	13.6	ND	3.0
10Cu-303-4h	9.8	309	7.7	ND	2.9
10Cu-353-4h	9.9	302	12.4	ND	2.8
10Cu-4h	9.9	294	15.7	ND	2.2
20Cu-303-4h	19.7	381	6.8	4.5	3.0
20Cu-353-4h	19.6	382	10.7	4.8	3.5
20Cu-4h	19.5	409	10.8	ND	2.8
20Cu-16h	19.6	414	11.0	4.5	2.5
20Cu-24h	19.5	406	9.9	4.7	3.1
20Cu-40h	19.6	421	10.5	ND	3.3
30Cu-4h	29.0	480	8.6	3.6	3.0
40Cu-4h	37.2	558	6.2	3.8	3.0

[a]Metal loading was determined by ICP-OES. [b]Diameter of Cu particles calculated from the XRD data by the Scherrer equation. [c]ND = not detected.

Cu Species Characterization. To investigate the reaction, the surface amounts of Cu^0 and Cu^+ sites must be qualitatively and quantitatively measured sequentially. Thus, all of the reduced Cu/SiO_2 catalysts were characterized by N_2O titration, X-ray photoelectron spectroscopy (XPS), X-ray Auger electron spectroscopy (XAES), and in situ Fourier transform infrared spectroscopy (FTIR) of CO absorption. The Cu^0 surface areas that were measured using N_2O titration are given in Table 2. With an increase in Cu loading, the surface area significantly varies from 5.0 to 44.2 $m^2\ g^{-1}$. For catalysts with identical Cu contents, $S_{Cu(0)}$ also significantly changes because of the modified aging procedures used during preparation. The XPS data (Figure 3a) show only two peaks, which are centered at binding energies of 932.0 and 951.8 eV, conventionally assigned to Cu^+ and Cu^0 species. The absence of a Cu 2p satellite peak at 942−944 eV strongly demonstrates that all Cu^{2+} species had been reduced to a low valence state of +1 or 0 after the reduction. Furthermore, the appearance of two obvious

DOI: 10.1021/acscatal.5b01678
ACS Catal. 2015, 5, 6200−6208

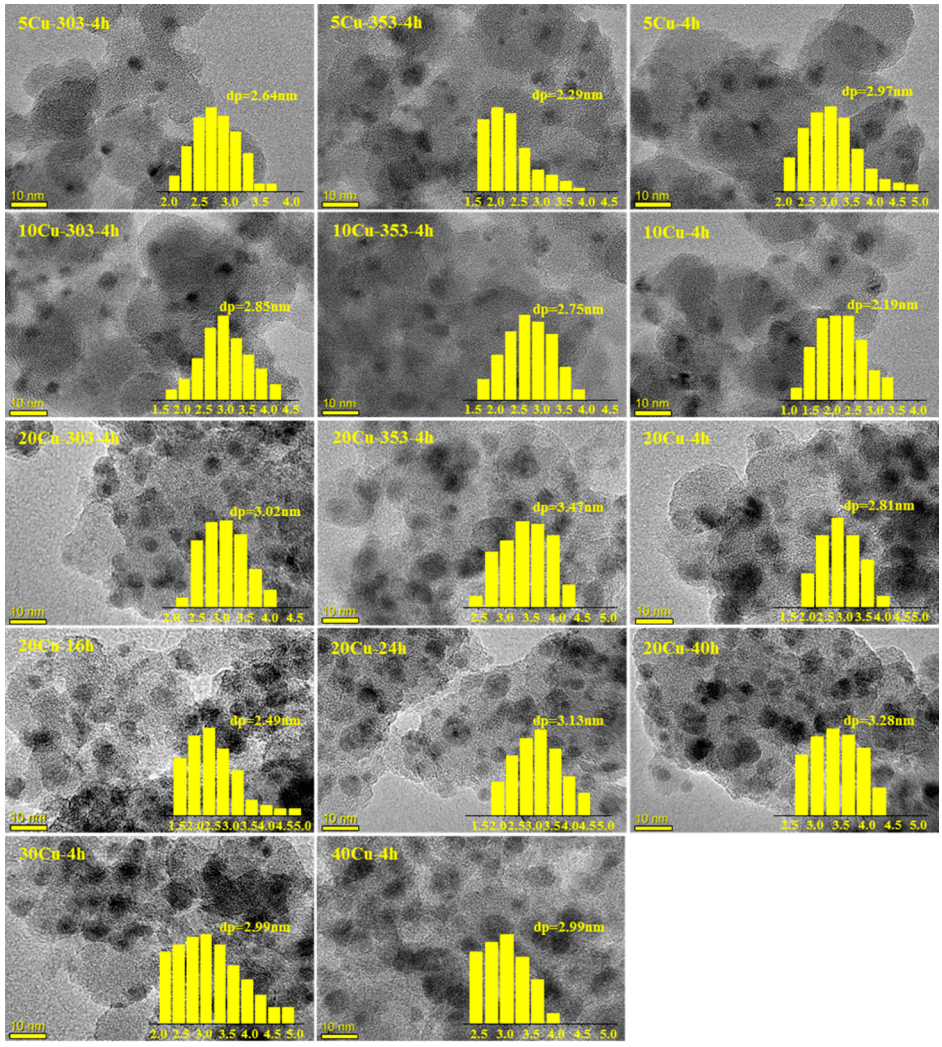

Figure 1. TEM images of the reduced catalysts.

overlapping peaks at 569.9 and 573.0 eV in the Cu LMM Auger electron spectra (Figure 3b) can be employed to distinguish between Cu^0 and Cu^+ species. From the deconvolution results, the molar ratios of the surface $Cu^+/(Cu^0 + Cu^+)$, which is denoted $X_{Cu(I)}$, are apparently affected by changes in the preparation conditions. Assuming that the Cu^+ ions and Cu^0 atoms occupy identical areas and have identical atomic sensitivity factors, the Cu^+ surface area can be estimated on the basis of Cu^0 surface area and $X_{Cu(I)}$.[26] This value was calculated and is given in Table 2 as $S_{Cu(I)}$, which obviously changes in contrast with $S_{Cu(0)}$.

To verify the specific surface areas of Cu species using a third method, the Cu/SiO_2 catalysts were characterized by in situ FTIR of CO adsorption (Figure 3c). Considering the weak interaction between CO and Cu^0 or Cu^{2+} species and the fact that it has been proved that no Cu^{2+} species exist after reduction by both XPS and XRD data, the obtained bands at 2100−2200 cm^{-1} should be attributed to CO adsorbed on Cu^+ species.[27,28] The bands at 2122 cm^{-1} should be assigned to the associated Cu^+ species.[29,30] As shown in Figure 3c, the intensity of bands at 2122 cm^{-1} generally increased with increasing Cu loading. Moreover, the proportion of integral areas under the peak at 2122 cm^{-1} displayed an opposite trend with the amount of copper phyllosilicate in calcined catalysts (see detail in Figure S1 in the Supporting Information), which has been proven to be helpful in Cu dispersion. In this case, the broad band around 2190 cm^{-1} should be attributed to CO-adsorbed isolated Cu^+ species. Deconvolution of the band allows us to see that there are two peaks at around 2197 and 2173 cm^{-1}. It has been reported that Cu^+ possesses two coordinative vacancies and can coordinate one or two CO molecules to form monocarbonyls or dicarbonyls, which explain the two peaks.[29,31] The bands at 2197 and 2173 cm^{-1} are attributed to the isolated Cu^+ species in dicarbonyls and monocarbonyls, respectively.[29,32] The integral areas of the Cu^+-CO peaks after normalization are given in Table 2; these integral areas are consistent with the $S_{Cu(I)}$ values (Figure S2 in the Supporting Information). This consistency check confirms that the qualitative and quantitative measurements of the Cu^0 and Cu^+ surface areas are accurate and reliable, which establishes a solid foundation for further investigations.

Catalytic Performance. To find the proper distribution of Cu species that enhances the catalytic performance, the vapor-phase hydrogenation of MA was performed as a probe reaction over these reduced Cu/SiO_2 catalysts. Correlating the MA conversion and the distribution of Cu species, we observed several interesting results. For example, in the case of the 20Cu-*x*h catalysts, the catalytic activities perfectly changed according to the number of Cu^+ sites, while the $S_{Cu(0)}$ values remained approximately constant. This result is in agreement with recent

DOI: 10.1021/acscatal.5b01678
ACS Catal. 2015, 5, 6200−6208

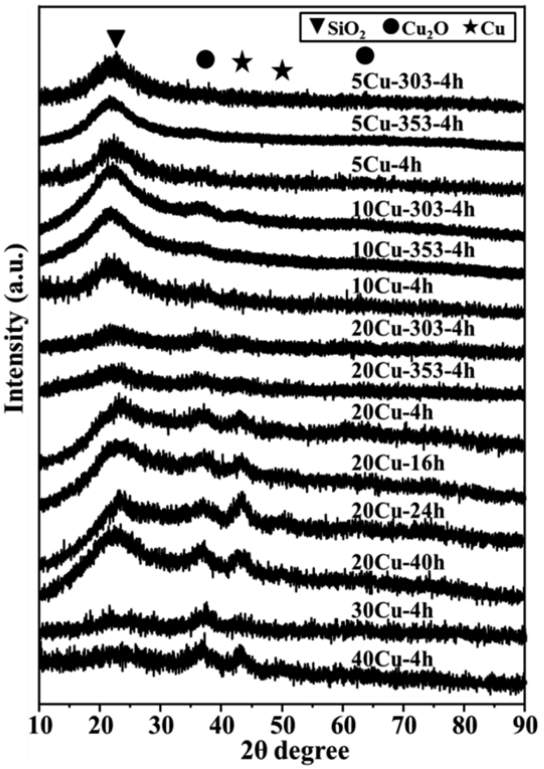

Figure 2. XRD patterns of reduced catalysts.

reports from Yuan and co-workers, who suggested that cuprous species acted as efficient active sites to activate acyl groups and the maximum amount of Cu^+ led to the greatest catalytic activities (see examples in Figure S3a in the Supporting Information).[14,21−23,30] However, in the case of the catalysts with 10 wt % Cu loadings and the 5Cu-303-4h sample, all of which exhibited similar surface areas of Cu^+ species but significant differences in Cu^0 surface areas, a different trend was observed. The catalytic activities no longer remained consistent with $S_{Cu(I)}$ but primarily increased with the Cu^0 surface area, which is also supported by numerous studies (see examples in Figure S3b in the Supporting Information).[14,17,20,33] On the basis of this discussion, the catalytic activity of these controllable prepared Cu/SiO_2 catalysts is concluded to undergo complex changes in the hydrogenation reactions. Therefore, it is necessary to establish a full-range relationship between the catalytic performance and Cu species.

All of the results indicate that the catalytic performance of hydrogenation establishes a linear correlation with the Cu^0 and Cu^+ surface areas in different segments. For the convenience of discussion, the results are divided to two different parts according to different relationships between the surface area of the Cu species and the catalytic performance (Figure 4). Part I consists of the data for the 5 and 10 wt % Cu loaded catalysts, whose the Cu^0 surface areas are less than 20 m^2/g. The catalytic activities scale linearly with the accessible metallic Cu surface areas but are independent of Cu^+ surface area. Part II consists of the results from the remaining catalysts, whose $S_{Cu(0)}$ values are 22.1−44.2 m^2/g and the catalytic activities and Cu^+ surface areas exhibit a good linear correlation. The scatters indicate that neither $S_{Cu(0)}$ nor $S_{Cu(I)}$ can solely explain the changes in catalytic performance. In general, Cu^0 and Cu^+ active sites both play indispensable roles in the hydrogenation; however, they apparently compete to exert a dominant effect on the catalytic ability, which is responsible for the contradictory opinions from different investigators. Thus, further exploration of the precise roles of Cu species in the reaction is essential to understanding the balancing effect of Cu sites on the enhancement of hydrogenation.

Roles of Cu^0 and Cu^+ Species in Hydrogenation Reactions. Poels and Brands[13] have suggested that the Cu^0 species activates H_2 while the Cu^+ species adsorbs methoxy and acyl species in ester hydrogenation; however, no convincing evidence has been presented. The debate has been focused on the essentiality of cuprous species functions. Because the adsorption of ethyl acetate on Cu under reduction conditions has been hypothesized to proceed via the cleavage of the C−O bond adjacent to the carbonyl group,[34] we propose that the adsorption of aliphatic esters also proceeds in this manner. In the case of MA, the products of the reaction consist of CH_3C^*O and CH_3O^* species, which indicates that the methanol dissociative adsorption likely reflects the ester dissociative adsorption.[4] Herein, the in situ FTIR of methanol

Table 2. Characterization of Cu Species on Reduced Cu/SiO_2 Catalysts

catalyst	$S_{Cu(0)}$ (m^2/g)[a]	$X_{Cu(I)}$ (%)[b]	$S_{Cu(I)}$ (m^2/g)[c]	$A_{Cu(I)}$ (area/g)[d]
5Cu-303-4h	5.0	64.2	8.9	199.7
5Cu-353-4h	11.2	19.2	6.9	156.9
5Cu-4h	7.6	46.6	6.7	132.2
10Cu-303-4h	12.0	41.8	8.6	167.1
10Cu-353-4h	19.9	28.7	8.0	162.3
10Cu-4h	18.6	31.3	8.5	160.5
20Cu-303-4h	23.1	42.4	17.0	474.5
20Cu-353-4h	39.6	19.2	9.4	239.0
20Cu-4h	24.4	29.7	10.3	250.3
20Cu-16h	23.9	36.6	13.8	366.9
20Cu-24h	22.1	48.1	20.5	498.5
20Cu-40h	23.5	38.7	14.8	430.1
30Cu-4h	37.6	24.4	12.2	269.8
40Cu-4h	44.2	23.9	13.9	363.3

[a]Metallic Cu surface area determined by N_2O titration. [b]$Cu^+/(Cu^+ + Cu^0)$ calculated from Cu LMM XAES spectra. [c]Cu(I) surface area estimated on the basis of $S_{Cu(0)}$ and $X_{Cu(I)}$ under the assumption that the Cu^+ ions and Cu^0 atoms occupy identical areas and have identical atomic sensitivity factors. [d]Integral area under the peaks in the FTIR spectra of CO adsorption on active Cu(I) on the surface of catalysts after evacuation.

DOI: 10.1021/acscatal.5b01678
ACS Catal. 2015, 5, 6200−6208

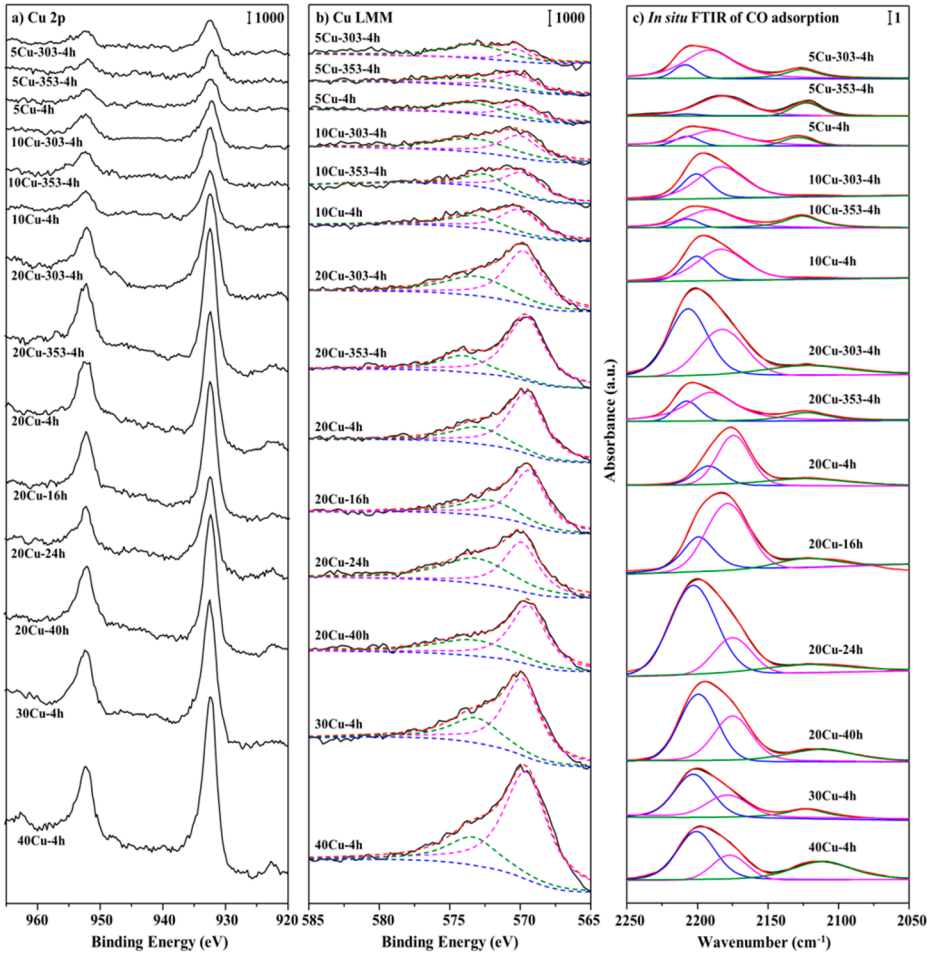

Figure 3. (a) XPS spectra, (b) XAES spectra, and (c) in situ FTIR of CO adsorption spectra of the reduced catalysts.

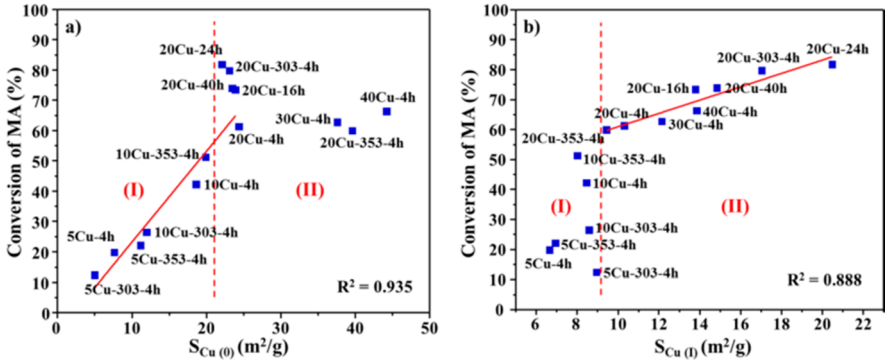

Figure 4. Balancing effect of Cu^0 and Cu^+ on the catalytic performance: correlation of the MA conversions with (a) Cu^0 surface areas and (b) Cu^+ surface areas.

adsorption was further applied to validate the important role of Cu^+ species on ester activation. It has been demonstrated that the IR bands at 2813 and 2924 cm^{-1} are attributable to the asymmetric and symmetric C−H stretching vibrations of Cu^0-OCH_3, respectively.[35] Additionally, the bands at 2856 and 2957 cm^{-1} have been assigned to the asymmetric and symmetric C−H stretching vibrations of methoxy species chemisorbed on a silica support.[35] However, we propose that these two peaks also include the C−H stretching vibration of methoxy species chemisorbed on Cu^+ species. As shown in Figure 5, the peaks at 2813 and 2924 cm^{-1} disappear when the desorption temperature is increased to 488 K, whereas the intensities of the bands at 2856 and 2957 cm^{-1} decrease only slightly. The bands at higher wavenumbers can be reasonably assigned to a stronger methoxy adsorption, which is presumed to be the Cu^+-OCH_3 species. Under this assumption, we integrated and normalized the areas of different peaks for comparison with the surface areas of both Cu^0 and Cu^+ species to determine whether the Cu^+ species act as the methoxy adsorption sites. The correlations in Figure S4 in the Supporting Information establish an excellent linear fit between the integral areas and the surface areas of the corresponding active sites. Moreover, the changes in intercepts of the fitting of the peaks at 2856 and 2957 cm^{-1} can be explained by a blank test with the SiO_2

DOI: 10.1021/acscatal.5b01678
ACS Catal. 2015, 5, 6200−6208

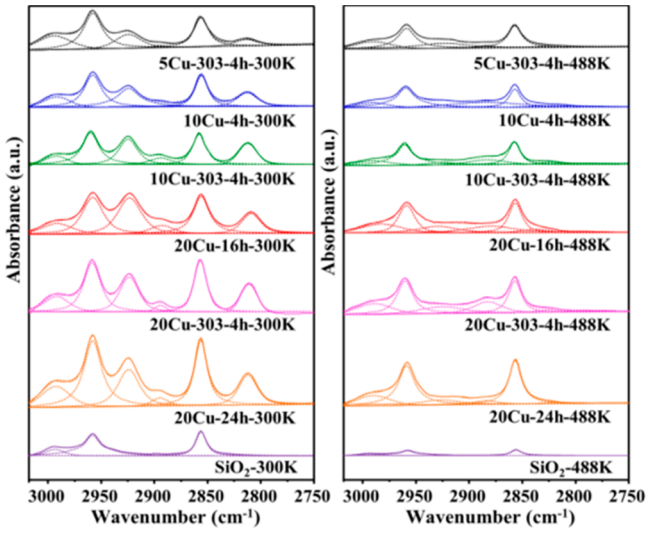

Figure 5. In situ FTIR spectra of methanol adsorption at 300 and 488 K.

support, which shows that the methoxy species are chemisorbed onto silica at 300 K but only slightly at 488 K. These results mutually confirmed the validity of the band assignment and Cu^+ function for ester activation. Hence, the Cu^+ sites contribute to the adsorption of methoxy and acyl species of esters during the hydrogenation reactions, while Cu^0 species cannot adsorb methoxy at the experimental reaction temperature.

A series of density functional theory (DFT) calculations was employed here as well to further identify the active roles of Cu^0 and Cu^+ species (see the Supporting Information for details). In the DFT calculations, the optimized $Cu^{\delta+}/SiO_2$ structures were modeled as Cu^+ sites because the accommodation and stabilization of cuprous species benefit from the strong interaction between Cu and supports. Owing to the diffraction peak at a 2θ angle of 43.3° in the XRD pattern and the observed lattice fringes in TEM images, which are attributed to metallic Cu(111), the Cu(111) plane structure was selected to represent the Cu^0 species. The processes of MA adsorption and H_2 decomposition were calculated on models of both Cu^0 and Cu^+ species, respectively. For the MA adsorption, the results show that the formation of CH_3O- and activation of the acyl group of MA are facilitated on $Cu^{\delta+}/SiO_2$ structures (see Table S2 in the Supporting Information), whereas it is almost impossible for the activation to happen on the Cu(111) plane (see Table S3 in the Supporting Information). For the H_2 decomposition, the activation energy calculation results indicate that decomposition occurs much more easily on Cu(111) (see Figure S10 in the Supporting Information). Thus, according to the DFT calculation results, the Cu^+ sties likely adsorb methoxy and acyl species since it is difficult to activate the ester on the metallic Cu species, while Cu^0 facilitates the decomposition of H_2. These inferences are consistent with the deductions from the in situ FTIR of methanol adsorption.

DISCUSSION

According to the results obtained above, both Cu^0 and Cu^+ active sites play indispensable roles in the hydrogenation and they compete against each other to exert a dominant effect on the catalytic ability. Thus, there is a equilibrium problem between the amouts of Cu^0 and Cu^+ species for obtaining the best catalytic performance. Here, we combine the TOFs of each Cu species and the precise roles analyzed above to elucidate the balancing effect of the active sites in hydrogenation reactions.

Analyzing the catalytic performance on the surface area of each Cu species will provide further understanding of the contributions of Cu^0 and Cu^+ species toward the hydrogenation reactions. The $TOF_{Cu(0)}$ and $TOF_{Cu(I)}$ values were calculated; the results are shown in Figure 6. The samples were divided into two parts, the same as in Figure 4. As shown in part I, the catalytic performance independently changes with the Cu^+ surface area but linearly increases with an increasing number of Cu^0 sites when the metallic Cu surface area is below a certain value (approximately 20 m^2/g). This result is consistent with the hypothesis that the maximum Cu^0/Cu^+ ratio exhibits the best performance, where the experiments were performed using catalysts with low metallic Cu surface areas (1.6−11.7 m^2/g). Given the role of Cu^0 sites, this relationship may originate from insufficient H_2 decomposition, which limits the reaction rates. On the other hand, the catalytic activity linearly increases with increasing Cu^+ surface area in part II, where the samples have relatively high Cu^0 surface areas. This trend is in agreement with reports that the maximum number of Cu^+ sites corresponds to the highest catalytic activity, when a series of catalysts were prepared using various methods and exhibited high $S_{Cu(0)}$ values (21.3−49.1 m^2/g). In this case, we deduce that the effect of Cu^+ on the catalysts starts to emerge when the H_2 decomposition is sufficient. In addition, the catalytic performance increases with both the Cu^+ surface area and the Cu^0 surface area (Figure 6b, part II). We inferred that the relative space position of the two types of active Cu sites may play an important role in the catalytic performance. Increasing

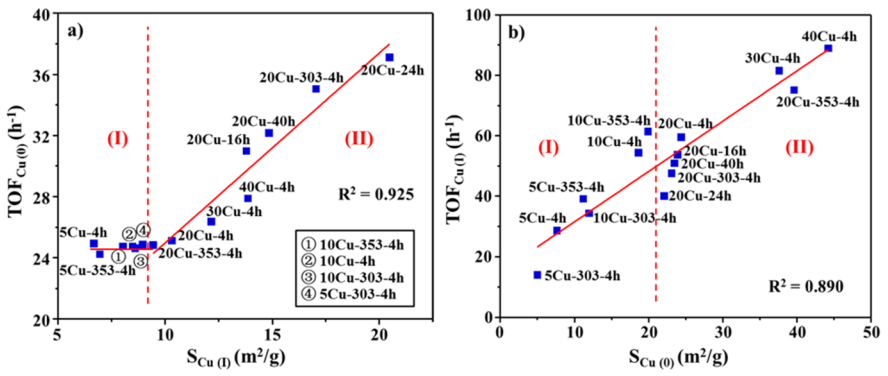

Figure 6. Effects of (a) Cu^+ active sites and (b) Cu^0 active sites on the catalytic performance, respectively.

DOI: 10.1021/acscatal.5b01678
ACS Catal. 2015, 5, 6200−6208

the accessible surface area of cuprous species undoubtedly improves the amount of active sites adjacent to metallic Cu species, which may result in the sustained growth of $TOF_{Cu(I)}$. Therefore, when the amount of Cu^0 species present is insufficient, the catalytic activity of hydrogenation is determined by the activity of H_2, whereas it is most strongly affected by the adsorption of methoxy and acyl species. The two types of Cu species demonstrate a balancing effect on enhancement of the catalytic performance in C−O hydrogenation reactions.

In addition to Cu^+ species, numerous kinds of Lewis acidity sites have been reported recently exhibiting promoting effects on homogeneous and heterogeneous catalysis in the hydrogenation of amides and other derivatives of carboxylic acids.[36−39] Hardacre and co-workers[36] suggested Ti^{3+} Lewis acid species weakened the C═O bond of the carbonyl oxygen of the acid and promoted hydrogenation and carbon−oxygen bond cleavage in TiO_2-supported Pt−Re catalysts for hydrogenation of carboxylic acids to fatty alcohols. Beller et al.[37] reported the Lewis acid and water activation of the catalyst in toluene and the novel selective C−OH bond cleavage of hemiacetal intermediates. The concepts described in all these papers for very different systems are essentially identical with our results. Actually, the Lewis acid activation effects on esters and other carbonyl moieties are quite general phenomena. The balancing effect of active species reported here have the potential to contribute to an understanding of the catalytic essence of hydrogenation of polar moieties in both homogeneous and heterogeneous catalysis.

CONCLUSION

In summary, using multiple and mutually corroborated characterizations, we observed 14 Cu/SiO_2 catalysts with high comparability due to their full-range distribution of Cu species and similar general morphologies. This comparability enabled us to trace the differences in activity of the samples to the contributions of both Cu^0 and Cu^+ species in C−O hydrogenation reactions. When the accessible metallic Cu surface area was below a certain value, the catalytic activity of hydrogenation linearly increased with increasing Cu^0 surface area, whereas it was primarily affected by the Cu^+ surface area. The obtained results are consistent with the available literature data and present a complete picture of the balancing effect of these two active Cu sites on enhancing the catalytic performance, where the Cu^+ sties adsorb methoxy and acyl species and Cu^0 facilitates the decomposition of H_2. It is indicated that when the amount of Cu^0 species is insufficient, the catalytic activity of hydrogenation is determined by the activity of H_2, whereas it is most affected by the adsorption of methoxy and acyl species. The controversy regarding the precise roles of active Cu sites in the hydrogenation is resolved, and the potential to make new progress in studies of the C−O hydrogenation mechanism has been demonstrated. Furthermore, new possibilities have been introduced for the rational design of catalysts through a modular approach with relevant functional chemicals in accord with a deep understanding of the contribution of active sites toward the reaction.

ASSOCIATED CONTENT

Supporting Information

The Supporting Information is available free of charge on the ACS Publications website at DOI: 10.1021/acscatal.5b01678.

Catalytic performance data, supplementary analysis, and details of DFT calculations (PDF)

AUTHOR INFORMATION

Corresponding Author

*X.M.: e-mail, xbma@tju.edu.cn; fax, +86-22-87401818; tel, +86-22-27409248.

Notes

The authors declare no competing financial interest.

ACKNOWLEDGMENTS

This research was supported by the National Natural Science Foundation of China (91434127, 21325626, 21276186).

REFERENCES

(1) Filonenko, G. A.; Aguila, M. J. B.; Schulpen, E. N.; van Putten, R.; Wiecko, J.; Müller, C.; Lefort, L.; Hensen, E. J. M.; Pidko, E. A. *J. Am. Chem. Soc.* **2015**, *137*, 7620−7623.

(2) Kelley, P.; Lin, S.; Edouard, G.; Day, M. W.; Agapie, T. *J. Am. Chem. Soc.* **2012**, *134*, 5480−5483.

(3) Ren, Y. L.; Yan, M. J.; Wang, J. J.; Zhang, Z. C.; Yao, K. S. *Angew. Chem., Int. Ed.* **2013**, *52*, 12674−12678.

(4) Santiago, M. A. N.; Sanchez-Castillo, M. A.; Cortright, R. D.; Dumesic, J. A. *J. Catal.* **2000**, *193*, 16−28.

(5) Goldemberg, J. *Science* **2007**, *315*, 808−810.

(6) Yue, H. R.; Zhao, Y. J.; Ma, X. B.; Gong, J. *Chem. Soc. Rev.* **2012**, *41*, 4218−4244.

(7) Huber, G. W.; Shabaker, J. W.; Dumesic, J. A. *Science* **2003**, *300*, 2075−2077.

(8) Pritchard, J.; Filonenko, G. A.; van Putten, R.; Hensen, E. J. M.; Pidko, E. A. *Chem. Soc. Rev.* **2015**, *44*, 3808−3833.

(9) Yue, H. R.; Ma, X. B.; Gong, J. L. *Acc. Chem. Res.* **2014**, *47*, 1483−1492.

(10) Deutsch, K. L.; Shanks, B. H. *J. Catal.* **2012**, *285*, 235−241.

(11) Zhu, Y. F.; Kong, X.; Li, X. Q.; Ding, G. Q.; Zhu, Y. L.; Li, Y. W. *ACS Catal.* **2014**, *4*, 3612−3620.

(12) San, X.; Zhang, Y.; Shen, W.; Tsubaki, N. *Energy Fuels* **2009**, *23*, 2843−2844.

(13) Poels, E. K.; Brands, D. S. *Appl. Catal., A* **2000**, *191*, 83−96.

(14) Gong, J. L.; Yue, H. R.; Zhao, Y. J.; Zhao, S.; Zhao, L.; Lv, J.; Wang, S. P.; Ma, X. B. *J. Am. Chem. Soc.* **2012**, *134*, 13922−13925.

(15) Yue, H. R.; Zhao, Y. J.; Zhao, S.; Wang, B.; Ma, X. B.; Gong, J. L. *Nat. Commun.* **2013**, *4*, 2339.

(16) Natesakhawat, S.; Lekse, J. W.; Baltrus, J. P.; Ohodnicki, P. R.; Howard, B. H.; Deng, X.; Matranga, C. *ACS Catal.* **2012**, *2*, 1667−1676.

(17) Yin, A.; Guo, X.; Dai, W. L.; Fan, K. *J. Phys. Chem. C* **2009**, *113*, 11003−11013.

(18) Yin, A.; Guo, X.; Fan, K.; Dai, W.-L. *ChemCatChem* **2010**, *2*, 206−213.

(19) Yin, A.; Guo, X.; Dai, W. L.; Li, H.; Fan, K. *Appl. Catal., A* **2008**, *349*, 91−99.

(20) Wen, C.; Yin, A.; Cui, Y.; Yang, X.; Dai, W. L.; Fan, K. *Appl. Catal., A* **2013**, *458*, 82−89.

(21) Zhao, S.; Yue, H. R.; Zhao, Y. J.; Wang, B.; Geng, Y. C.; Lv, J.; Wang, S. P.; Gong, J. L.; Ma, X. B. *J. Catal.* **2013**, *297*, 142−150.

(22) He, Z.; Lin, H.; He, P.; Yuan, Y. *J. Catal.* **2011**, *277*, 54−63.

(23) Zheng, X.; Lin, H.; Zheng, J.; Duan, X.; Yuan, Y. *ACS Catal.* **2013**, *3*, 2738−2749.

(24) Huang, Y.; Ariga, H.; Zheng, X.; Duan, X.; Takakusagi, S.; Asakura, K.; Yuan, Y. *J. Catal.* **2013**, *307*, 74−83.

(25) Wang, Y. N.; Duan, X.; Zheng, J.; Lin, H.; Yuan, Y.; Ariga, H.; Takakusagi, S.; Asakura, K. *Catal. Sci. Technol.* **2012**, *2*, 1637−1639.

(26) Chen, L. F.; Guo, P. J.; Qiao, M. H.; Yan, S. R.; Li, H. X.; Shen, W.; Xu, H. L.; Fan, K. N. *J. Catal.* **2008**, *257*, 172−180.

(27) Hadjiivanov, K.; Knozinger, H. *Phys. Chem. Chem. Phys.* **2001**, *3*, 1132−1137.

DOI: 10.1021/acscatal.5b01678
ACS Catal. 2015, 5, 6200−6208

(28) Hadjiivanov, K.; Venkov, T.; Knözinger, H. *Catal. Lett.* **2001**, *75*, 55−59.
(29) Hadjiivanov, K.; Kantcheva, M.; Klissurski, D. *J. Chem. Soc., Faraday Trans.* **1996**, *92*, 4595−4600.
(30) Lin, H.; Zheng, X.; He, Z.; Zheng, J.; Duan, X.; Yuan, Y. *Appl. Catal., A* **2012**, *445-446*, 287−296.
(31) Kuroda, Y.; Yoshikawa, Y.; Kumashiro, R.; Nagao, M. *J. Phys. Chem. B* **1997**, *101*, 6497−6503.
(32) Hadjiivanov, K.; Klissurski, D. *React. Kinet. Catal. Lett.* **1991**, *44*, 229−235.
(33) Yin, A.; Guo, X.; Fan, K.; Dai, W. L. *Appl. Catal., A* **2010**, *377*, 128−133.
(34) Kohler, M. A.; Cant, N. W.; Wainwright, M. S.; Trimm, D. L. *Chem. Inst. Can.* **1988**, 1043.
(35) Zhang, R.; Sun, Y.; Peng, S. *Fuel* **2002**, *81*, 1619−1624.
(36) Manyar, H. G.; Paun, C.; Pilus, R.; Rooney, D. W.; Thompson, J. M.; Hardacre, C. *Chem. Commun.* **2010**, *46*, 6279−6281.
(37) Li, Y.; Topf, C.; Cui, X.; Junge, K.; Beller, M. *Angew. Chem., Int. Ed.* **2015**, *54*, 5196−5200.
(38) Zhang, Y.; MacIntosh, A. D.; Wong, J. L.; Bielinski, E. A.; Williard, P. G.; Mercado, B. Q.; Hazari, N.; Bernskoetter, W. H. *Chem. Sci.* **2015**, *6*, 4291−4299.
(39) Jiang, Y.; Huang, W.; Schmalle, H. W.; Blacque, O.; Fox, T.; Berke, H. *Organometallics* **2013**, *32*, 7043−7052.

DOI: 10.1021/acscatal.5b01678
ACS Catal. 2015, 5, 6200−6208